Kinetic Role of Electrostatic Interactions in the Unfolding of Hyperthermophilic and Mesophilic Rubredoxins†

Silvia Cavagnero,‡,§ Derek A. Debe,‡ Zhi H. Zhou,|| Michael W. W. Adams,|| and Sunney I. Chan*,‡

Arthur Amos Noyes Laboratories of Chemical Physics, California Institute of Technology, Pasadena, California 91125, and Department of Biochemistry and Center for Metalloenzyme Studies, University of Georgia, Athens, Georgia 30602

Received September 3, 1997

ABSTRACT: The temperature dependence of the unfolding kinetics of rubredoxins from the hyperthermophile *Pyrococcus furiosus* (RdPf) and the mesophile *Clostridium pasteurianum* (RdCp) has been studied. Results show that RdPf unfolds much more slowly, under all experimentally accessible temperature regimes, than RdCp and other typical mesophilic proteins. Rates of RdCp and RdPf unfolding decrease upon increasing the pH above 2 and diverge dramatically at pH 7. As shown by detailed electrostatic energy calculations, this is the result of a differential degree of protonation of the negatively charged amino acids, which causes distinct electrostatic configurations as a function of pH. We propose that ion pairs, particularly those that are placed in key surface positions, may play a kinetic role by mildly clamping the protein and thereby influencing the nature and the number of the vibrational normal modes that are thermally accessible upon unfolding. More generally, these modes are also likely to be affected by the favorable electrostatic configurations, which we have shown to be directly linked to the extremely slow unfolding rates of RdPf at neutral pH. Even at pH 2, in the absence of any salt bridges, the unfolding rates of RdPf are much smaller than those of RdCp. This is ascribed to presently unidentified structural elements of nonelectrostatic nature. Since electrostatic effects influence the unfolding kinetics of both mesophilic and thermophilic rubredoxins, these findings may be of general significance for proteins.

Nature has equipped proteins with an organized three-dimensional structure that enables them to perform important biological functions, which include signaling, transport, and catalysis. These require a machinery with a considerable degree of conformational flexibility, which can only be achieved by reversible breakage/formation of relatively weak noncovalent interactions, triggered by small energetic inputs. It is not surprising, then, that the thermodynamic stability of proteins is only moderate, and it does not usually exceed 15 kcal/mol, with melting temperatures typically ranging between 40 and 60 °C. A less well understood situation occurs in the case of a selected number of microorganisms, commonly referred to as hyperthermophiles, that have the peculiar ability to thrive at temperatures ranging from 80 to 110 °C. Most hyperthermophiles are classified as *Archaea* (*1*), and they live in the vicinity of submarine hydrothermal vents and continental hot springs or solfataric fields. Proteins from these life forms are obviously distinct from the more conventional mesophilic organisms, which typically live only up to about 40 °C. Optimal growth temperatures for various organisms may serve as a rough indication of the expected lower limits to the melting temperatures of their respective proteins. While it is not entirely clear, at present, what causes the exceptional *in vivo* and *in vitro* thermostability displayed by the proteins produced by hyperthermophiles, it is known that heat resistance does not minimally compromise their ability to efficiently perform catalytic and transport functions (*2*). Whether the thermodynamic stability of these proteins at their physiological temperatures is higher than that of their mesophilic counterparts has not been firmly established to date. Initial studies suggest that there may be no general answer to this question. Investigations performed on Sso7d from *Sulfolobus solfataricus* (*3*) indicate that this protein has an only moderate mesophilic-like intrinsic thermodynamic stability. Its peculiarly high melting temperature arises from a rather shallow and low-intensity stability curve (*4*) with a broad free-energy maximum spanning a wide temperature range. In contrast to these findings, more recent studies performed on a hyperthermophilic rubredoxin suggest that the thermodynamic stability of this protein exceeds that of typical mesophilic proteins (*5*). On the other hand, the kinetic properties of proteins from hyperthermophiles have not until now been explored.

An excellent model system for the study of the unusual properties of hyperthermophilic proteins is the iron protein rubredoxin from *Pyrococcus furiosus* (RdPf),[1] a microorganism with an optimal growth temperature of 100 °C (*1*, *6*). RdPf is stable for prolonged periods *in vitro* upon boiling in aqueous buffer at pH close to neutral, and it unfolds only at temperatures well beyond 100 °C (*7*). Complete protonation of the negatively charged amino acids, at low pH, generates a fully folded structure with a somewhat lower

† This work was supported by NIH Grant Nos. GM 22432 (S.I.C.) and GM 50736 (M.W.W.A.) from the National Institute of General Medical Sciences, U.S. Public Health Service.

* To whom correspondence should be addressed.

‡ California Institute of Technology.

§ Present Address: Department of Molecular Biology MB-2, The Scripps Research Institute, 10550 North Torrey Pines Road, La Jolla, CA 92037.

|| University of Georgia.

S0006-2960(97)02179-X CCC: $15.00
Published on Web 02/18/1998

apparent melting temperature (*8*). The overall structural features of RdPf both in solution and in the crystalline form are very similar to those of rubredoxins from mesophilic organisms, except for a small number of extra ion pairs and hydrogen bonds (*9*, *10*).

We chose to focus our attention on RdPf and its mesophilic counterpart, rubredoxin from *Clostridium pasteurianum* (RdCp). The latter protein rapidly unfolds at 80 °C (*11*) at neutral pH, and both its biochemistry (*11*) and its structure (*12*−*14*) have been well-characterized. The present study focuses on the peculiar kinetic features that characterize the unfolding of hyperthermophilic proteins. We have determined unfolding activation parameters by measuring rate constants as a function of temperature. Furthermore, we have studied how electrostatic interactions modulate the unfolding kinetics.

MATERIALS AND METHODS

Protein Preparation. RdPf has been isolated and purified as previously described (*6*). Rubredoxin from *C. pasteurianum* (*13*, *14*) was purchased from Sigma. Concentrated stock solutions of the two proteins were used for the experiments described below. All pH values were determined at room temperature. Solution pH was checked before and after each experiment and found to be identical in each case, within experimental error.

Absorption Spectroscopy. The kinetics of unfolding were monitored by UV−vis absorption spectroscopy, with a Hewlett-Packard 8452A single-beam diode-array spectrophotometer. Full spectra were recorded per each time point. Spectra were typically analyzed at 380 nm. A 1 cm quartz cuvette was used. The temperature was controlled via a Haake D1 thermostated water bath connected to the compartment surrounding the cuvette housing. The experiments were performed in aqueous buffer under vigorous stirring at different temperatures. Buffer solutions were placed in the spectrophotometer cuvette and allowed to reach thermal equilibrium at the desired temperature. The temperature of the solution inside the cuvette was carefully measured with a resistor sensor. After the buffer solution had reached thermal equilibrium, a concentrated RdPf solution was rapidly added and spectral acquisition started. The dead time of this apparatus, inclusive of the time required for mixing and, supposedly, temperature equilibration, is 1−2 s. In all cases this time was negligible compared to the lifetime of the species undergoing unfolding. No denaturing agents were employed. Buffers consisted of 40 mM glycine solutions at pH 2.0 or 2.7 and 40 mM tris(hydroxymethyl)-aminomethane or 3-(*N*-morpholino)propanesulfonate solutions at pH 7.0. All of the spectroscopic data were baseline-corrected. This was done for each time point by subtracting experimental absorbances from the corresponding absorbances at 700 nm, where no contribution is expected from RdPf transitions.

Data Analysis. The absorption spectra were analyzed on an IBM-compatible computer, with the software package Lab Calc (Galactic Industries Corporation). Nonlinear least-squares curve fitting was done on a Macintosh computer with the program Kaleidagraph (Synergy Software). The following expression was used to fit the data recorded at 380 nm

$$OD_{OBS} = OD_0 \exp[-kt] + a \quad (1)$$

where OD_{OBS} represents the observed absorption signal, OD_0 is the absorption signal at time zero, and t is the time. The unfolding rate constant k and the constant a, which has been introduced to account for small baseline errors, have been treated as adjustable parameters.

The temperature dependence of unfolding rate constants has yielded activation parameters for each observed kinetic phase. The Arrhenius equation

$$k = A e^{\frac{-E_a}{RT}} \quad (2)$$

(*15*) was used to obtain preexponential factors (A) and activation energies (E_a). T, k, and R represent the absolute temperature, the observed kinetic rate constant, and the universal gas constant, respectively. Linear regression analysis was applied to $\ln(k)$ vs $1/T$ plots. The slopes and y-axis intercepts of these plots yielded E_a and A, according to eq 1. $\Delta H^{\ddagger}$ and $\Delta S^{\ddagger}$ were obtained from the slope and y-axis intercept of $\ln(k/T)$ vs $1/T$ plots. Linear fits were analyzed according to the Eyring equation

$$k = \frac{\kappa k_B T}{h} e^{\frac{+\Delta S^{\ddagger}}{R}} e^{\frac{-\Delta H^{\ddagger}}{RT}} \quad (3)$$

(*16*), where κ is the transmission coefficient, k_B is the Boltzmann constant, and h is the Planck constant. A value of 1 was used for κ. Finally, activation free energies ($\Delta G^{\ddagger}$) of Table 1 were obtained by directly solving the Eyring equation in the following form:

$$k = \frac{\kappa k_B T}{h} e^{\frac{-\Delta G^{\ddagger}}{RT}} \quad (4)$$

Electrostatic Free-Energy Calculations. Electrostatic free-energy calculations have been performed with the program DELPHI (*17*; Biosym Technologies Inc.). Details of the method of finite differences have been discussed elsewhere (*18*). The protein was treated with a dielectric of 4, embedded in water solvent of dielectric constant 80. Hydrogen atoms were built onto crystal structures of RdPf (1caa.bkv) and RdCp (5rxn.bkv) prior to electrostatic calculations using the Biograph program (Molecular Simulations Inc.) and AMBER (*19*) bond and angle parameters. Separate structures were constructed, representing each pH 2 and 7 configuration. No partial charges were used. Unit charges were placed at the centers of the N and O charged atoms. A solvent accessible surface probe of 1.4 Å was used (*20*). An

[1] Abbreviations used: RdPf, rubredoxin from *Pyrococcus furiosus*; RdCp, rubredoxin from *Clostridium pasteurianum*; Lyz, lysozyme; Brom, stem bromelain; Tryp, trypsin; Trp Syn, α-subunit of Trp synthase; CI2, chymotrypsin inhibitor 2; T, absolute temperature; R, universal gas constant; k, observed kinetic constant; k_{unf}, unfolding rate constant; $t_{1/2}$, unfolding half-life; κ, transmission coefficient; k_B, Boltzmann constant; h, Planck's constant; A, Arrhenius preexponential factor; E_a, Arrhenius activation energy; $\Delta H^{\ddagger}$, unfolding activation enthalpy; $\Delta S^{\ddagger}$, unfolding activation entropy; $\Delta G^{\ddagger}_{unf}$, unfolding activation free energy; E_{El}, electrostatic free energy; E_{Coul}, Coulomb free energy; E_{Sol}, solvation free energy; ΔE_{Coul}, difference in E_{Coul} between pH 7 and pH 2; ΔE_{Sol}, difference in E_{Sol} between pH 7 and 2; q, total protein charge; Δq_{add}, number of negative charges added upon raising the pH from 2 to 7; Δq_{net}, difference in net charge upon raising the pH from 2 to 7.

Table 1: Estimated Unfolding Rate Constants (k_{unf}), Half-Lives ($t_{1/2}$), and Activation Free Energies ($\Delta G^{\ddagger}_{unf}$) of RdPf and Some Mesophilic Proteins at 100 °C[a]

protein	exptl condns	k_{unf} (s^{-1})	$t_{1/2}$ (s)	$\Delta G^{\ddagger}_{unf}$ (kcal/mol)
tryptophan synthase[b] (α-subunit)	pH 7.8, 0 M GnCl[c]	0.35	2	23
stem bromelain[d]	pH 3.4	$1.2 \times 10^{+3}$	6×10^{-4}	17
trypsin[e]	pH 2	$1.4 \times 10^{+4}$	5×10^{-5}	15
lysozyme[f]	pH 2.6, 0.7 M GnCl	$1.2 \times 10^{+2}$	6×10^{-3}	19
chymotrypsin inhibitor 2[g]	pH 6.3, 0 M GnCl[c]	69	10^{-2}	19
RdCp	pH 2.0	$3.5 \times 10^{+2}$	2×10^{-3}	18
RdCp	pH 7.0	3.9×10^{-3}	$1.8 \times 10^{+2}$	26
RdPf	pH 2.0	2.3	0.3	21
RdPf	pH 2.7	5.8×10^{-3}	$1.2 \times 10^{+2}$	26
RdPf	pH 7[h]	1.9×10^{-6}	$3.7 \times 10^{+5}$	32

[a] Linear extrapolations to 100 °C have been performed on the original data, which were acquired in the experimentally accessible temperature ranges at 1 atm pressure. $\Delta G^{\ddagger}_{unf}$ values have been derived by introducing k_{unf} values into the Eyring eq 4 and solving it for $\Delta G^{\ddagger}_{unf}$. [b] Reference 22. [c] Extrapolated from GnCl concentration dependence studies. [d] Reference 24. [e] Reference 26. [f] Reference 23. [g] Reference 25. [h] Deduced from pH dependence studies (see Figure 3, curve 5).

atomic radius of 1.3 Å for the iron center was added to the bond lengths provided by the program DELPHI.

RESULTS

The present studies indicate that RdPf unfolds much more slowly than RdCp, under similar experimental conditions. Additionally, RdPf unfolding rates are much more sensitive to pH variations than the corresponding RdCp rates. This suggests that particular electrostatic configurations of RdPf are responsible for the observed kinetic effects. A detailed analysis of our results follows.

Unfolding Rates of Mesophilic and Hyperthermophilic Proteins. Thermal unfolding of RdPf and RdCp has been initiated by a temperature-jump induced by manual mixing. The process has been followed in real time by absorption spectroscopy. In the temperature range that has been analyzed (62−96 °C), the unfolding rates of RdPf for the step involving Fe^{3+} loss are extremely slow (see the accompanying paper (*21*) for a detailed description of the RdPf unfolding mechanism). Figure 1 shows the temperature dependence of the time-decay of the Cys → M charge-transfer absorption bands of RdPf at pH 2.0. The curves follow monoexponential kinetics, which suggest that Fe^{3+} is lost in a single step. First-order rate constants are readily obtained (Table 1), and the corresponding Eyring plot (*16*) gives an excellent fit (Figure 1b). A comparison between RdPf unfolding rates and the available published data for the unfolding of mesophilic proteins is presented in Figure 2. It is apparent that the unfolding rates of RdPf are considerably slower than those of the nonthermophilic proteins for which kinetic data are available: tryptophan synthase (*22*), lysozyme (*23*), stem bromelain (*24*), chymotrypsin inhibitor 2 (*25*), and trypsin (*26*). To ensure more meaningful comparison among different proteins, some of the original data from the literature have been extrapolated to 0 M guanidine hydrochloride concentration. This was only possible in cases where the authors had studied the guanidine hydrochloride dependence of the kinetic parameters (*22*, *25*). A rough estimate of the differences in unfolding rates between RdPf and the mesophilic proteins of Figure 2 is readily obtained by extrapolating the RdPf curve to a temperature range relevant to mesophilic proteins, i.e., at values ranging from 20 to 80 °C. This procedure reveals that RdPf unfolds more slowly than typical mesophilic proteins by at least 2 orders of magnitude, in a mesophilic environment.

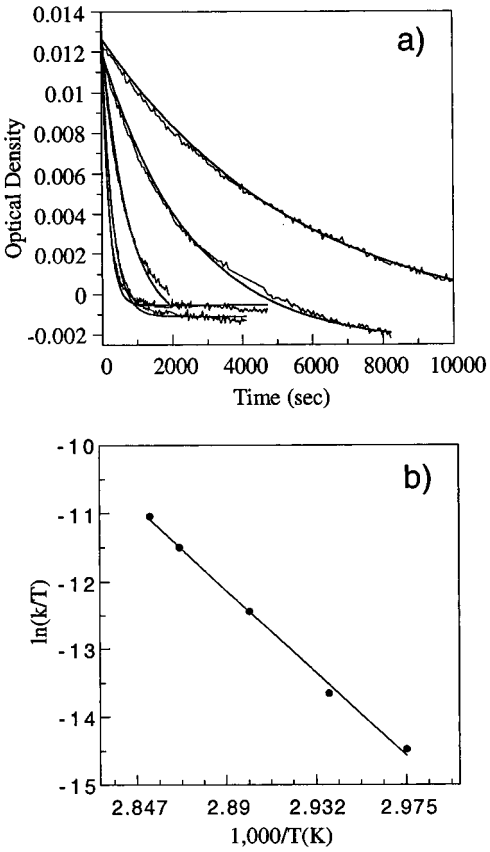

FIGURE 1: Temperature dependence of RdPf unfolding kinetics as followed by UV−vis absorption spectroscopy at 380 nm, pH 2.0. (a) Kinetic traces with corresponding monoexponential curve fits. The temperature for the different traces was as follows going from the upper to the lower trace: 62.4, 66.6, 71.0, 75.5, 76.7 °C. First-order rate constants were determined by nonlinear regression analysis, assuming a two-state model. (b) Eyring plot.

It is important to note that our kinetic data derive only from measurements of the unfolding kinetic step involving iron loss. However, results presented in the accompanying paper (*21*) indicate that this step, although intrinsically very slow, is not the rate-determining step of the unfolding process. The rate-determining step is even slower and it occurs later during unfolding. This further supports our results and suggests that the rate of iron loss defines an upper

Table 2: Activation Parameters for Rubredoxin Unfolding, According to Both Arrhenius and Transition-State Theory[a]

protein	E_a (kcal mol^{-1}) (exptl error)	A (s^{-1}) (exptl error)	$\Delta H^{\ddagger}$ (kcal mol^{-1}) (exptl error)	$\Delta S^{\ddagger}$ (cal mol^{-1} deg^{-1}) (exptl error)
RdPf, pH 2.0	61 (3)	4×10^{36} (4×10^{36})	60 (3)	101 (7)
RdPf, pH 2.7	74	5×10^{40}	73	125
RdCp, pH 2.0	51 (2)	4×10^{33} (4×10^{33})	50 (2)	88 (7)
RdCp, pH 7.0	49 (5)	2×10^{32} (2×10^{32})	49 (5)	60 (12)

[a] E_a, A, $\Delta H^{\ddagger}$, and $\Delta S^{\ddagger}$ denote Arrhenius activation energies, preexponential factors, unfolding activation enthalpies, and unfolding activation entropies, respectively. Experimental errors are expressed as standard deviation of the mean.

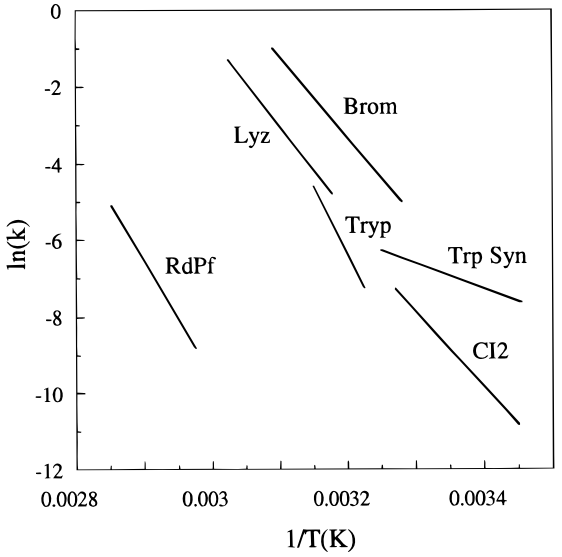

FIGURE 2: Arrhenius plots for the unfolding of RdPf and a few mesophilic proteins. RdPf, pH 2, as probed by absorption spectroscopy at 380 nm: Lyz, lysozyme, 0.7 M GnCl and pH 2.6; Brom, stem bromelain, pH 3.4; Tryp, trypsin, pH 2; Trp Syn, α-subunit of Trp synthase, pH 7.8, the original data have been extrapolated to 0 M GnCl; CI2, chymotrypsin inhibitor 2, pH 6.3, data extrapolated to 0 M GnCl.

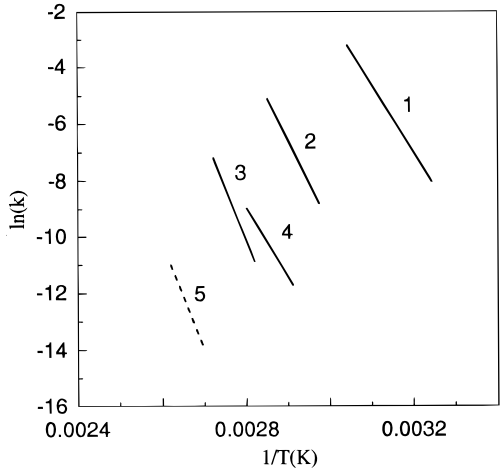

FIGURE 3: Arrhenius plots for the unfolding of RdPf and RdCp at different pH values: (1) RdCp, pH 2.0; (2) RdPf, pH 2.0; (3) RdPf, pH 2.7; (4) RdCp, pH 7.0; (5) RdPf, hypothetical curve projected to pH 7 (dotted curve). Experimental curves are the result of the study of the temperature dependence of the unfolding kinetics by absorption spectroscopy at 380 nm. Curve 5 does not represent the predicted behavior of RdPf at pH 7, but rather, it is intended to suggest upper limits to the expected unfolding rates of this protein at pH 7. Curve 5 has been constructed according to the criteria described in the Results.

limit to the intrinsic unfolding rates. RdPf unfolding was irreversible, under our experimental conditions. The unfolding kinetics were wavelength independent over the entire wavelength range of absorption by the charge-transfer bands.

As shown, the mesophilic protein data of Figure 2 have been collected by different investigators. Small inevitable differences in the experimental conditions (i.e., pH, ionic strength, etc.) used for each of these proteins and RdPf make rate comparisons less than ideal. A more quantitatively meaningful unfolding analysis of hyperthermophilic and mesophilic proteins is obtained by directly assessing the temperature dependence of the unfolding kinetics for RdPf and its mesophilic counterpart, rubredoxin from *C. pasteurianum* (RdCp). These data for both proteins have been collected under the same carefully controlled conditions. Arrhenius curves (*15*) for these processes are shown in Figure 3. Over the experimentally accessible temperature range, the observed unfolding rates constants for the two proteins at pH 2 differ by a factor of about 3×10^3, RdPf being the more slowly unfolding protein. This difference is quite remarkable, considering that the two metalloproteins share the same tertiary fold and have very similar three-dimensional structural features (*9*, *10*). The expected half-life ($t_{1/2}$) of RdPf extrapolated to 100 °C is 0.3 s, i.e., about 2 orders of magnitude greater than that of RdCp, at pH 2.0 (Table 1). This result highlights the intrinsic kinetic stability of RdPf over its mesophilic counterpart. The above is true despite the fact that protonation of all the RdPf titratable amino acids in a low pH environment (*8*) leads to electrostatic destabilization (Table 3). Under these conditions and in a high-temperature environment, RdPf still retains a competitive advantage over its mesophilic counterpart.

Table 3: Calculated Coulomb Free Energies (E_{Coul}) and Solvation Free Energies (E_{Sol}) of RdPf and RdCp as a Function of pH[a]

protein	pH	E_{Coul}	ΔE_{Coul}	q	Δq_{add}	Δq_{net}	E_{Sol}	ΔE_{Sol}
RdPf	7.0	99.2	−83.2	−8	−14	2	−2242.7	−1127.1
RdPf	2.0	182.4		+6			−1115.6	
RdCp	7.0	550.6	431.0	−12	−17	7	−3770.3	−2926.8
RdCp	2.0	119.6		+5			−843.5	

[a] The energy differences for the various terms between pH 7 and 2 are indicated as ΔE_{Coul} and ΔE_{Sol}. The total protein charge is expressed as q, and the number of negative charges added to the system as pH is raised from 2 to 7 is denoted Δq_{add}. The difference in net charge in going from pH 2 to 7 is expressed as Δq_{net}. Energies have been calculated at 298 K. Values are expressed as multiples of kT. All the calculations have been performed with the program DELPHI (*17*).

pH Dependence of Unfolding Rates. The pH dependence of the unfolding rates of RdPf and RdCp as a function of temperature (Figure 3) reveals that, as the pH is increased, the Arrhenius curves keep approximately the same slope but shift to the left, implying slower unfolding rates at a given temperature. This applies to both hyperthermophilic and

mesophilic rubredoxins. Similar slopes do suggest that kinetic differences between these proteins are to be ascribed to preexponential factors only. However, this is not entirely substantiated by our data, since even subtle changes in slope are sufficient to produce sizable variations in activation energies. All the Arrhenius plots in Figure 3 are linear in the experimentally tested temperature range. This implies that the unfolding activation enthalpies ($\Delta H^{\ddagger}$) do not depend on temperature. As a consequence, there are negligible changes in activation heat capacity between the native states and the unfolding transition states of RdPf and RdCp.

In the case of RdCp, the Arrhenius curve shift in going from pH 2 to 7 is quite pronounced. Similarly, the corresponding plot for RdPf moves to the left upon varying the pH from 2 to 2.7. This change in pH accounts for the protonation of a single negatively charged amino acid, based on the electrometric pH titration curve of RdPf (*8*). At pH greater than 2.7, RdPf unfolding rates become too slow to be reliably measured at experimentally accessible temperatures. Therefore, for technical reasons, it was not possible to obtain a complete set of pH-dependent Arrhenius curves for RdPf. The available data show that the RdPf curve shifts to the left, upon varying the pH from 2.0 to 2.7, by about one-half of the shift undergone by the RdCp curve as the pH is changed from 2.0 to 7.0. Additionally, we have found that RdPf can be boiled for an indefinite amount of time, on the order of days, at neutral pH without losing its properties (data not shown). These observations indicate that RdPf unfolding rates are much more sensitive to the deprotonation of ionizable residues than RdCp rates. Our data also imply that unfolding rates of RdPf are dramatically slower that those of RdCp, at neutral pH. A hypothetical unfolding Arrhenius curve for RdPf at neutral pH (Figure 3, curve 5) has been constructed by applying an unfolding rate shift similar to that experienced by RdCp upon varying the pH from 2 to 7. This curve simply establishes approximate upper limits to the expected unfolding rates of RdPf at pH 7, and it has obviously nothing to do with the actual Arrhenius profile of the protein at neutral pH, which may be further shifted to the left by an unspecified amount. This is due to the fact that the sensitivity of RdPf to electrostatic effects is greater than that of RdCp, as discussed above. Table 1 shows that the expected upper limit to the unfolding rate of RdPf at pH 7 and 100 °C is 1.9×10^{-6} s^{-1}. The corresponding lower limit to the unfolding half-life ($t_{1/2}$) under the same conditions is $3.7 \times 10^{+5}$ s, i.e., about 102.8 h. This number is presumably compatible with the lifetime of cells of *P. furiosus* in its natural environment, e.g., cells have a doubling time of about 40 min at 100 °C under laboratory conditions (*27*), and it is consistent with the observed *in vitro* thermostability of RdPf at the optimal growth temperature of this microorganism.

To confirm the validity of our results, we have repeated the unfolding experiments a number of times to estimate the experimental uncertainties associated with the data collected under similar experimental conditions. In general, the data collected at higher pH were affected by greater uncertainties, presumably because unfolding gets exceedingly slow (up to several days at the temperatures that we have studied) as the pH is raised. Very slow processes are less likely to be highly reproducible.

Activation Parameters. The unfolding activation parameters for RdPf and RdCp, according to Arrhenius and transition-state theory, are presented in Table 2. They generally have greater magnitude in the case of RdPf. Furthermore, sizable increases in both activation energies and preexponential factors characterize the unfolding of RdPf, upon going from pH 2 to 2.7. In the case of RdCp, on the other hand, activation energies do not appreciably vary but the preexponential factors get lower, as the pH is raised from 2 to 7. Corresponding variations take place when activation enthalpies ($\Delta H^{\ddagger}$) and entropies ($\Delta S^{\ddagger}$) are considered. All the observed $\Delta S^{\ddagger}$ values are large and positive. Although our data do not show it explicitly, monotonic variations of unfolding rates with pH are very likely between the experimentally tested pH values. This is consistent with what has generally been observed in the literature (*23*, *26*).

Electrostatic Free Energy Studies. Electrostatic interactions are entirely responsible for the changes undergone by a protein with pH (*28*). The overall secondary and tertiary structures of RdPf undergo only minimal variations as the pH is lowered from 7 to 2 (*8*). This suggests that the observed slower unfolding rates of RdPf compared to RdCp at low pH's are to be ascribed to subtle, and consequently hard to pinpoint, structural effects. Obviously, this consideration also applies to the previously observed (*8*) variations in apparent melting temperatures.

We have performed some electrostatic free-energy calculations in order to estimate whether the rate effects presented in this work would correlate to pH-dependent thermodynamic changes. We have calculated the expected variations in the electrostatic free energy (E_{El}) of RdPf and RdCp between pH 2 and 7. Our calculations have assumed that contributions arise only from fully ionizable residues. This approximation is acceptable for qualitative purposes, and it gives reliable results to first order. The electrostatic free energy of a protein is given by the sum of its Coulomb free energy (E_{Coul}) and its solvation free energy (E_{Sol}) components:

$$E_{El} = E_{Coul} + E_{Sol} \tag{5}$$

The DELPHI program has been used to derive values for E_{Coul} and E_{Sol}. The calculation involves solving the Poisson−Boltzmann equation for the electrostatic potential and subsequently converting the results into energies. E_{Sol} is calculated as the difference in reaction field energy between an in solvent and an in vacuo calculation. It is important to note that, because of uncertainties associated with the choice of the water and protein dielectric constants, the absolute values of the energies here should only be used to highlight trends. In addition, precise calculations of the solvation term in the pH 2 states are subject to slight structural differences in the proteins between the pH 2 and the pH 7 states, which are unknown at this time. On the other hand, since small structural fluctuations have less effect on the Coulomb contribution, relative pH-dependent variations within E_{coul} can be relied upon with confidence.

Results from Table 3 show that (i) the E_{Coul} term of RdPf at pH 7 is considerably smaller than the corresponding term of RdCp, (ii) the stabilization energy ΔE_{Coul} of RdPf from pH 2 to 7 is also smaller and it has opposite sign to the ΔE_{Coul} term for RdCp, and (iii) solvation energies of both proteins increase upon decreasing the pH (i.e., the ΔE_{Sol} term

is negative). Observations i and ii reflect the fact that the overall charge configuration of RdPf is much more stable than that of RdCp. This is due to both the presence of additional salt bridges and to the more uniform charge distribution of RdPf. The high E_{coul} value of RdCp at neutral pH is ascribed to the prominent separation of opposite charges on relatively distant surface regions and to heavy negative charge clustering. The latter effect can be visually assessed by inspection of the published GRASP (*29*) images of RdCp (*8*). The negative sign of the RdPf ΔE_{Coul} term as pH is lowered from 7 to 2 is due to the disappearance of the charge neutralization effect as all the negatively charged groups get protonated. On the other hand, the positive sign of the RdCp ΔE_{Coul} term as pH goes from 7 to 2 is a consequence of the increasingly smaller degree of opposite-charge separation. This results in like-charge clustering due to the progressive disappearance of negative charge from the protein surface. The data for the Coulombic term clearly underline the thermodynamic relevance of the peculiar charge distribution and of the ion pairs in RdPf. However, particularly in the case of ion pairs, it is not possible to directly infer that these interactions confer extra stability to RdPf, since the solvation energy term (E_{Sol}), being proportional to the protein net charge (see Table 3), exhibits compensatory effects.

DISCUSSION

The nature of the differences between proteins from hyperthermophilic and mesophilic organisms is not well understood to date. While most studies that have appeared so far have concentrated on comparing structural (*8*, *30*) and thermodynamic (*4*, *5*) features, this paper shows that RdPf and RdCp, each produced by one of the two classes of organisms, display very distinct kinetic properties. As seen in the Results, our data indicate that the unfolding kinetics of RdPf is considerably slower than in the case of several mesophilic proteins (Figure 2), including RdCp (Figure 3, Table 1). More specifically, the unfolding half-lives of RdPf and RdCp differ by 2 orders of magnitude at pH 2. At this pH value all of the acidic residues of RdPf have been protonated (*8*), all of its salt bridges have been disrupted, and the presence of net (positive) charge repulsion is reflected by the high value of the electrostatic free energy (Table 3). The fact that RdPf still retains slower unfolding kinetics, as well as a considerably higher apparent melting temperature (*8*) than RdCp, clearly indicates that there is a component due to forces of nonelectrostatic nature that is contributing to the kinetic, and possibly the thermodynamic, stability of RdPf at low pH. These forces are almost certain to be present at neutral pH as well. Our absorption measurements at 380 nm monitor the electronic environment of the Fe^{3+} coordination site. However, it is unlikely that the observed differences in the kinetic behavior of RdPf and RdCp are a direct consequence of structural variations in the metal ion core of the two proteins since this has a similar geometry in RdPf and RdCp (*10*, *13*, *14*). This view is supported by the fact that an extremely slow unfolding kinetics has also been observed for the RdPf unfolding steps that do not involve the metal ion to any extent (*21*). Thus, noncovalent contributions due to the polypeptidic portion of the protein are likely to play an important role as well. Although these forces are yet to be identified, they are very likely hydrophobic in origin, due to their persistence in the presence of very different RdPf electrostatic configurations. A recent comparison of the structures of RdPf and RdCp suggested that the hydrophobic energy associated with the protein fold might be stronger in the case of RdPf (*31*). Further insights into their nature are given by a comparison of the unfolding activation parameters of RdPf and RdCp at pH 2 (Table 2). Both the activation energy E_a and the preexponential factor A of RdPf are higher than those of RdCp at this pH. However, while E_a is only 16% higher, A is larger by as much as about 3 orders of magnitude. A discussion of the implications of these kinetic results is beyond the scope of this study and will be the subject of a future publication.

The unfolding of both RdPf and RdCp gets slower as the pH is raised. This enhances the differences between RdPf and RdCp, since the kinetic behavior of RdPf at pH 2.7 is similar to that of RdCp at neutral pH. Although it has not been possible so far to measure the precise unfolding kinetic parameters of RdPf at neutral pH, our data suggest that its unfolding half-life is very long, and it amounts to at least 102 h (Table 1 and Figure 3) under these conditions. Dramatic increases in activation parameters are also implied by the trend manifested in going from pH 2 to 2.7. The increase in both E_a and A, as well as the increase in both $\Delta H^{\ddagger}$ and $\Delta S^{\ddagger}$, for RdPf, upon increasing the pH from 2 to 2.7, is fully consistent with either the creation of a salt bridge or a more generally stable electrostatic configuration. In accordance with this, calculations done on the native state show that both the Coulomb and the solvation components of the electrostatic free energy of RdPf decrease as pH increases (Table 3). Because of the uncertainties associated with the E_{Sol} term discussed in the previous section, it is not possible to quantify the electrostatic free energy component of RdPf as a function of pH. However, the trend displayed by both the E_{Coul} and E_{Sol} terms for RdPf indicates that E_{El} is lower at higher pH values, i.e., the protein is more thermodynamically stable at higher pH. This poses the interesting question of whether the large rate deceleration effects observed for the protein as pH increases can be entirely accounted for by variations in the free energies of the native state or whether, and if so, to what extent, the different pH-dependent electrostatic changes also affect the properties of the unfolding transition state. The electrostatic calculations presented here only refer to the native state and offer no clues about the energetic or the detailed electrostatic configuration of the unfolding transition state.

Regardless of the origin of hyperthermostability of RdPf, we emphasize here that we have observed a direct correlation between the degree of thermostability of different rubredoxins and the magnitude of their observed unfolding activation free energies (Table 1). Specifically, hyperthermostability of a rubredoxin is accompanied by a higher activation free energy of unfolding from the native state. Whatever the molecular determinants of hyperthermostability, it is clear that they either stabilize the native state or destabilize the unfolding transition state, or both, such that in the case under study there is a dramatically enhanced kinetic barrier toward unfolding RdPf relative to RdCp.

In interpreting the observed pH dependence of the Arrhenius plots of both RdPf and RdCp, we have taken advantage of the fact that changes in pH can be correlated to the protonation state of the ionizable surface residues through

electrometric pH titration curves (*32*, *33*). We have also worked under the assumption that forces of nonelectrostatic nature are affected by pH changes to a much smaller extent than electrostatic forces. This view is corroborated by the fact that the experimental apparent melting temperature of RdPf decreases linearly with pH through protonation of all the negatively charged amino acid side chains, but it then flattens out at lower pH values (S. Cavagnero et al., unpublished results). In this connection, we note that, as ionic strength is increased, all surface charges become shielded. Furthermore, salt bridges are expected to get weaker, even at high pH, making it very hard to draw any conclusions. For this reason, we elected to maintain the ionic strength at the low value of 40 mM in all of our pH dependence studies. Another important point to be noted is that forces such as ion−dipole, dipole−dipole, dipole−induced dipole, and induced dipole−induced dipole are also electrostatic in origin (*34*). Additionally, hydrogen bonds are also believed to be of partially electrostatic nature (*34*). Therefore, all of these noncovalent forces are expected to display some pH dependence. Nonetheless, we assume that these interactions make a smaller contribution to the electrostatic energy than the ion pairs and classical monopole electrostatic interactions. We have obviously biased our calculations in this manner by selecting the appropriate charge parameters used in the electrostatic free-energy calculations presented here.

There has been much discussion in the literature about the general role of ion pairs in a protein (*35*−*38*). It is currently believed that salt bridges contribute to the thermodynamic stability by only a small extent because of (a) the desolvation penalty that needs to be paid upon ion-pair formation and (b) to enthalpy−entropy compensation effects. In the specific case of RdPf, protonation of the negatively charged residues, which results in salt bridge disruption, lowers the apparent melting temperature by about 20 °C (*8*). However, data presented in Table 3 suggest that there might be a sizable contribution to this effect from simple charge neutralization. Thus, within the context of protein folding, ion pairs and, more generally, stable charge configurations resulting from uniform distributions of unlike charges, evidently play an important kinetic role that had not been pointed out before. It is conceivable that the very slow RdPf unfolding rates at neutral pH may result from a mild surface "clamping" effect exerted by the salt bridges on the native structure. By providing localized structural constraints in key positions on the protein surface, ion pairs restrict the number as well as the nature of the vibrational normal modes of the protein that can be thermally accessible and contribute to the energy flow that can lead to thermal unfolding of the protein. This could be the case for RdPf, as illustrated by Figure 4. The observed decreased unfolding rates need to be interpreted in this manner in our view. Since these concepts apply to both hyperthermophilic and mesophilic proteins alike, these effects may be of general significance in biochemistry.

Within the temperature range analyzed in this study, the Arrhenius plots of both RdPf and RdCp are linear, suggesting that there is no detectable heat capacity change in going from the native state to the activated complex (*39*). This supports the notion that the activated complex does not have a greater number of exposed hydrophobic groups than native RdPf

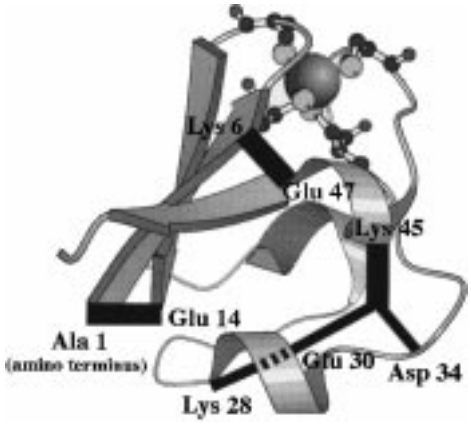

FIGURE 4: Ribbon diagram of RdPf based on the crystal structure (*10*) showing the main ion pairs of the protein. The sphere in the upper portion of the figure represents the Fe^{3+} center. Backbones and side chains of the four cysteine metal ligands are shown explicitly. The residues involved in salt bridge formation are labeled on the figure. Interactions resulting from ion pairs are depicted by solid black bands. The diagram was prepared using the program Molscript (*41*).

(*40*), a concept that is fairly in line with what has generally been found for other proteins (*23*, *26*).

It is possible that specific electrostatic interactions (as well as hydrophobic contacts) play a special role and affect the unfolding kinetics in a particular way. This issue has not been treated in this work, and it will be addressed in future studies based on thermodynamic analysis. While we have focused on kinetic analysis, future experimental efforts will also be directed toward clarifying the role that thermodynamics plays in the thermostabilization of proteins from hyperthermophilic life forms.

The present work has focused on the comparative analysis of hyperthermophilic and mesophilic protein unfolding kinetics. This is, to our knowledge, the first study that has addressed this issue. We have shown that the thermal unfolding of RdPf is several orders of magnitude slower than in the case of mesophilic proteins. The different pH dependence of thermal denaturation rates of RdPf and RdCp has provided insights into the kinetic role played by electrostatic interactions in proteins. It is clear that particular electrostatic configurations are able to affect unfolding kinetics by modulating both activation energies and preexponential factors. We have proposed that localized structural constraints due to electrostatic forces are able to slow RdPf unfolding by affecting the way the protein channels thermal energy from the solvent bath into those modes that ultimately soften those contacts that are part of the transition state in the unfolding process. The specific mechanisms by which this phenomenon may take place are currently under investigation.

We conclude with a brief discussion of the large preexponential factors (A) and activation energies (E_a or $\Delta H^{\ddagger}$) observed for the protein unfolding kinetics. Although the unfolding of a protein is effectively a unimolecular process, thermal energy must be channeled into the protein to activate the protein vibrational modes. In a protein solution, this is accomplished by the strong coupling between the protein vibrational modes and the large thermal bath which it is in contact with. If we make the simple assumption that the protein, P, can only begin to unfold when it has acquired a

threshold energy of activation, and this threshold is reached when state P* is populated, then we may denote the unfolding process by the following simple series of events

$$\mathrm{P} \overset{K_1}{\rightleftharpoons} \mathrm{P}^*$$

$$\mathrm{P}^* \overset{k_2}{\rightleftharpoons} \mathrm{U} \tag{6}$$

where K_1 is the equilibrium constant describing the population of P* and k_2 denotes the first-order rate constant for the unfolding of the protein from state P*. Within the context of this simple scheme, it is trivial to show that

$$k = K_1 k_2 = \kappa(k_B T/h)(e^{\Delta S_1/R})(e^{\Delta S_2^{\ddagger}/R})(e^{-\Delta H_1/RT})(e^{-\Delta H_2^{\ddagger}/RT}) \tag{7}$$

or

$$\Delta H^{\ddagger} = \Delta H_1 + \Delta H_2^{\ddagger}$$

$$\Delta S^{\ddagger} = \Delta S_1 + \Delta S_2^{\ddagger} \tag{8}$$

Thus, the measured $\Delta H^{\ddagger}$ and $\Delta S^{\ddagger}$ (or E_a and A) reflect both the enthalpy and entropy of formation of P* as well as the kinetic activation parameters associated with the unfolding of the protein from P*.

ACKNOWLEDGMENT

We thank Prof. Doug Rees and Dr. Reginald Waldeck for helpful discussions and critical comments on this work.

REFERENCES

1. Woese, C. R., Kandler, O., and Wheelis, M. L. (1990) *Proc. Natl. Acad. Sci. U.S.A. 87*, 4576−4579.
2. Adams, M. W. W. (1993) *Annu. Rev. Microbiol. 47*, 627−658.
3. Knapp, S., Karshikoff, A., Berndt, K. D., Christova, P., Atanasov, B., and Ladenstein, R. (1996) *J. Mol. Biol. 264*, 1132−1144.
4. Becktel, W. J., and Schellman, J. A. (1987) *Biopolymers 26*, 1859−1877.
5. Hiller, R., Zhou, Z. H., Adams, M. W. W., and Englander, S. W. (1997) *Proc. Natl. Acad. Sci. U.S.A. 94*, 11329−11332.
6. Blake, P. R., Park, J.-B., Bryant, F. O., Aono, S., Magnuson, J. K., Eccleston, E., Howard, J. B., Summers, M. F., and Adams, M. W. W. (1991) *Biochemistry 30*, 10885−10895.
7. Klump, H. H., Adams, M. W. W., and Robb, F. T. (1994) *Pure Appl. Chem. 66*, 485−489.
8. Cavagnero, S., Zhou, Z. H., Adams, M. W. W., and Chan, S. I. (1995) *Biochemistry 34*, 9865−9874.
9. Blake, P. R., Park, J.-B., Zhou, Z. H., Hare, D. R., Adams, M. W. W., and Summers, M. F. (1992) *Protein Sci. 1*, 1508−1521.
10. Day, M. W., Hsu, B. T., Joshua-Tor, L., Park, J.-B., Zhou, Z. H., Adams, M. W. W., and Rees, D. C. (1992) *Protein Sci. 1*, 1494−1507.
11. Lovenberg, W., and Sobel, B. E. (1965) *Proc. Natl. Acad. Sci. U.S.A. 54*, 193−199.
12. Watenpaugh, K. D., Sieker, L. C., and Jensen, L. H. (1979) *J. Mol. Biol. 131*, 509−522.
13. Watenpaugh, K. D., Sieker, L. C., Herriot, J. R., and Jensen, L. H. (1973) *Acta Crystallogr. B29*, 943.
14. Yasunobo, K. T., and Tanaka, M. (1983) in *Iron−Sulfur Proteins* (Lovenberg, W., Ed.) pp 27−130, Academic Press, New York.
15. Arrhenius, S. (1889) *Z. Phys. Chem. 4*, 226−248.
16. Eyring, H. (1935) *Chem. Rev. 17*, 226−248.
17. Nicholls, A., and Honig, B. (1991) *J. Comput. Chem. 12*, 435−445.
18. Sharp, K. A., and Honig, B. (1990) *Annu. Rev. Biophys. Chem. 19*, 301−332.
19. Cornell, W. A., Cieplak, P., Bayly, C. I., Gould, I. R., Merz, K. A., Ferguson, D. M., Spellmeyer, D. C., Fox, T., Caldwell, J. W., and Kollmann, P. A. (1995) *J. Am. Chem. Soc. 117*, 5179−5197.
20. Yang, A.-S., Gunner, M. R., Sampogna, R., Sharp, K., and Honig, B. (1993) *Proteins 15*, 252−265.
21. Cavagnero, S., Zhou, Z. H., Adams, M. W. W., and Chan, S. I. (1998) *Biochemistry 37*, 3377−3385.
22. Chen, X. W., and Matthews, C. R. (1994) *Biochemistry 33*, 6356−6362.
23. Segawa, S.-I., and Sugihara, M. (1984) *Biopolymers 23*, 2473−2488.
24. Arroyo-Reyna, A., and Hernandez-Arana, A. (1995) *Biochim. Biophys. Acta 1248*, 123−128.
25. Jackson, S. E., and Fersht, A. R. (1991) *Biochemistry 30*, 10436.
26. Pohl, F. M. (1968) *Eur. J. Biochem. 7*, 146−152.
27. Fiala, G., and Stetter, K. O. (1986) *Arch. Microbiol. 145*, 56−61.
28. Dill, K. A. (1990) *Biochemistry 29*, 7133−7155.
29. Nicholls, A., Sharp, K., and Honig, B. (1991) *Proteins: Struct., Funct., Genet. 11*, 281−296.
30. Richie, K. A., Teng, Q., Elkin, C. J., and Kurtz, D. M. (1996) *Protein Sci. 5*, 883−894.
31. Swartz, P. D., and Zahiye, T. (1996) *Biochemistry 35*, 13772−13779.
32. Tanford, C. (1961) *Physical Chemistry of Macromolecules*, Wiley and Sons: New York.
33. Tanford, C. (1962) *Adv. Protein Chem. 17*, 69−165.
34. Maitland, G. C., Rigby, M., Smith, E. B., and Wakeham, W. A. (1981) *Intermolecular Forces—Their Origin and Determination*, Oxford University Press, New York.
35. Daopin, S., Sauer, U., Nicholson, H., and Matthews, B. W. (1991) *Biochemistry 30*, 7142−7153.
36. Daopin, S., Nicholson, H., Baase, W. A., Zhang, X. J., Wozniak, B. W., and Matthews, B. W. (1991) *Ciba Found. Symp. 161*, 52−62.
37. Hendsch, Z. S., and Tidor, B. (1994) *Protein Sci. 3*, 211−226.
38. Sali, D., Bycroft, M., and Fersht, A. R. (1991) *J. Mol. Biol. 220*, 779−788.
39. Oliveberg, M., Tan, Y.-J., and Fersht, A. R. (1995) *Proc. Natl. Acad. Sci. U.S.A.* 92, 8926−8929.
40. Privalov, P. L., and Makhatadze, G. I. (1990) *J. Mol. Biol. 213*, 385−391.
41. Kraulis, P. J. (1991) *J. Appl. Crystallogr. 24*, 946−950.

BI9721795